

Determination of stationary region boundary in multiple reference frames method in a mixing system agitated by Helical Ribbon Impeller using CFD

Maryam Sanaie-Moghadam, Mansour Jahangiri*, Faramarz Hormozi

School of Chemical & Petroleum and Gas Engineering, Semnan University, Semnan, Iran

PAPER INFO

History:

Received 27 April 2014
Received in revised form
28 June 2014
Accepted 22 July 2014

Keywords:

CFD
MRF
Helical Ribbon
Impeller
Mixing
Non-Newtonian
fluid

ABSTRACT

The multiple reference frames (MRF) method is the most suitable method to simulate impeller rotation in mixing systems. Precise determination of stationary and moving zones in MRF method leads to accurate results in mixing performance. In this research, the entire volume of mixing system was divided into two zones. The kinetic energy values were used to distinguish the zones with different velocities. The low-velocity zones, close to zero, were considered as the stationary zone and higher velocities were considered as the moving zone. The standard geometrical parameters were used for mixing system. The axial velocity and axial flow number were compared with literatures for validation. The values for dimensionless diameter of stationary zone at different Reynolds numbers were achieved for Newtonian and non-Newtonian fluids that are in agreement with values applied in literatures. The results show that the dimensionless diameter of stationary zone decreases as Reynolds number increases.

© 2015 Published by Semnan University Press. All rights reserved.

1. Introduction

High viscosity mixing operations in agitated vessels are commonly encountered in chemical, biochemical, pharmaceutical, polymer, mineral, food, and wastewater treatment industries. Due to their ability to keep the entire vessel contents circulating, close-clearance impellers are very well suited to mixing high viscous liquids [1,2]. Among the close-clearance impellers, the helical ribbon impellers are recognized to be the most efficient systems. Because of their rather good homogenization potential caused by both tangential and axial motion, helical ribbon impellers are often used to agitate the high viscous mixtures of Newtonian or non-Newtonian fluids at low

Reynolds number. Jahangiri [3,4] studied the velocity profile, the local shear rate and the Metzner-Otto method for helical ribbon impeller using LDA for viscoelastic liquids in transitional region. Determination of power consumption and mixing times, under steady rotational speeds, for mixing systems equipped with close clearance impellers such as screw or helical ribbon agitators was investigated by Takahashi et al. [5], Carreau et al. [6] Delaplace et al. [7] and Ihejirika et al. [8]. The conventional evaluation of mixing is done through experiments with different impellers, vessel geometries, and fluid rheology. Patterson et al. [9] tested mixing performance of HRI (Helical Ribbon Impeller) on the Newtonian and non-Newtonian fluids by experimental methods. This approach is usually expensive, time consuming,

and difficult; moreover, the resulting empirical correlations are suitable only for the specific systems being investigated. During the last two decades, CFD has become an important tool for understanding the flow phenomena [10-12], developing new processes [13-15], and improving the existing processes [16]. Using CFD, one can examine various parameters of the process in a shorter time with low costs. Many researchers applied CFD to study mixing systems [17-19]. In the case of mixing systems, computational flow could have been easily achieved with multiple reference frames (MRF) [20], mixing plane method (MPM) or sliding meshes method (SMM). The simplest one is the MRF method proposed by Luo et al. [21]. The MRF method can be applied when the relative position between the impeller and baffle does not significantly affect the flow field due to weak interactions. While no baffle is applied, the MRF model is chosen to simulate the flow field generated by HR impeller in the stirred tank [22]. In order to use the MRF method, the calculation area should involve both stationary and moving zone. Accurate determination of boundary of these two zones results in a better mixing performance. In Zhang's research, as the classic MRF method, tank wall and impeller area are considered as stationary and moving zones, respectively, whereas Rahimiet al. [23] and Tsuiet al. [24] applied the different segmentation. Tsuiet al. [24] applied inner part of the vessel as the stationary zone and the outer part, where the helical blade impeller is located, as the moving zone. In their study, the interface between the two regions is nearly placed at half the distance between the inner edge of the blade and the shaft, but there was no reason represented for this choice. Rahimiet al. [23] used two different strategies to select the rotating volume. In the first MRF layout, a cylinder that surrounds the whole impeller was used as a moving frame that includes almost 80% of the fluid volume and the rest of the vessel was taken stationary. In the second MRF scheme, two regions in the central part of the vessel were treated as a stationary region. In this scheme, the vessel was divided into three stationary regions and one moving region. They achieved a better prediction of flow field with the second method. Again, no reason was represented for these choices.

In this study, it is shown that the position of interface between stationary and moving zones depends on the Reynolds number and fluid

type that can be determined using the kinetic energy values.

2. Model Development

2.1 CFD simulation

The mixing in the studied stirred tank was modeled using commercial CFD code, FLUENT 6.2. The entire computational domain was divided into several sub-domains to create the geometry. Unstructured tetrahedral mesh was used for moving zones including tank volume and impeller, also hexahedral meshes were used for the stationary zones including walls. The number of total cells is 235949. Figure 1 illustrates the mesh structure of mixing system. The finite volume method and a modified second-order scheme were applied to solve the Navier-Stokes equations and to discretize the governing equations to algebraic equations.

2.2 Assumptions

The steady state mixing flow was assumed in three-dimensional geometry. Water was chosen as the case for Newtonian and glycerin was chosen for Non-Newtonian fluid which are both isothermal and incompressible. The model is single-phase without any reaction. Based on the above assumptions, the governing equations are outlined as follows.

2.3 Continuity equation

The Continuity equation representing conservation of mass is expressed as:

$$\frac{\partial \rho}{\partial t} + \nabla \cdot (\rho U) = 0 \quad (1)$$

where ρ is the liquid density, and U is velocity vector

2.4 Momentum equation

Conservation of momentum is expressed as:

$$\frac{\partial \rho}{\partial t} (\rho U) + \nabla \cdot (\rho U U) = \rho g - \nabla P + \nabla \cdot (\tau) \quad (1)$$

where P is the static pressure, τ is the stress tensor, and ρg is the gravitational body force vector.

2.5 Mixing system

The helical ribbon impeller is centred in a flat-bottomed cylindrical tank with diameter of $D=0.276$ m, and liquid height of $H=0.21$ m. The

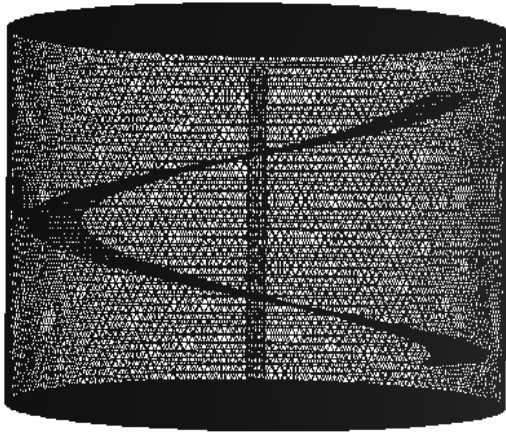


Fig. 1. Mesh structure of the mixing system.

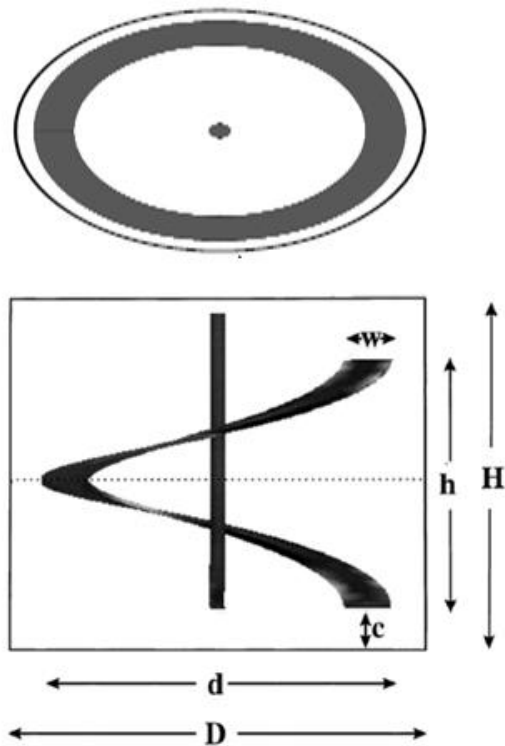


Fig.2.Mixing system.

diameter, height, width and thickness of the impeller are $d=0.255$ m, $h=0.14$ m, 3 mm and 1mm, respectively. The important dimensionless parameters governing the vessel are: $h/d = 0.549$, $w/d = 0.118$, and $D/d = 1.082$, where d , h , c , w and D , are the ribbon outer diameter, ribbon height, ribbon to wall clearance, ribbon width, and tank diameter, respectively. The schematic diagram is shown in Figure 2.

2.6 Boundary conditions

Since for Newtonian fluids, no vortex appears for rotational velocity below the 300rpm [25,26], the

free surface is defined as a symmetrical boundary condition for both Newtonian and non-Newtonian fluids where the normal velocity component is equal to zero. The no-slip condition is selected for the solid walls.

3. Validation

3.1 characteristics of flow field

Flow patterns enhanced by helical ribbon agitators have been studied by many researchers [8,13,23,24]. In spite of the different impeller geometries, the primary circulation patterns are approximately the same. Commonly, the liquid between the impeller and wall flows upwards (whilst simultaneously rotating), inwards along the surface, downwards in the core near the shaft and radially outwards near the bottom of the tank. The direction of this primary flow may be reversed by reversing the agitator rotation [16, 22].

In Fig.2 the basic flow pattern at the $Y=0$ plane of the stirred tank simulated in this work is consistent with the conclusion in Rahimi's work [23].

3.2Pattern of axial flow number

In order to validate the calculation methodology used in the present investigation, results have been compared with the case of Rahimi *et al.* [23] who reported computational axial flow number at different distances from the tank's bottom for a helical ribbon impeller. Both curves have the same pattern, but the values of axial flow number in Rahimi's work are greater than that of this work. This difference is due to inequality of aspect ratio (H/D). Higher aspect ratio of H/D results in greater value of axial velocity. Figure 4 shows a comparison of axial flow number in Rahimi's work

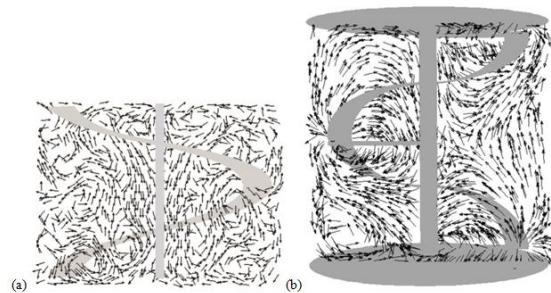


Fig.3. Tangential velocity vector map at $Y=0$ plane (a) Calculated by CFD in this work, $H/D=0.761$ (b) Calculated by Rahimiet al. [23], $H/D=1$.

with this work. The axial flow rate (Q_{ax}) has been found by the surface integration of the axial velocity component (positive v_z^+ or negative v_z^-) at various horizontal planes inside the vessel as follows:

$$Q_{ax}(z) = \int_A V_z^+ dA = \int_A V_z^- dA \quad (3)$$

in which A is the cell's radial surface area. Consequently, this average axial flow rate with ND^3 can be used to obtain the dimensionless axial flow number, N_{Qax} :

$$N_{Qax}(z) = \frac{Q_{ax}(z)}{ND^3} \quad (4)$$

In this study, the mixing performance in mixing system, described in section 2.5, was investigated at different Reynolds numbers for Newtonian and non-Newtonian fluids.

In stirred tanks, the Reynolds number (Re) was defined as follows:

$$Re = \frac{\rho Nd^2}{\mu} \quad (4)$$

in which N is the impeller rotational speed, d is the impeller diameter, ρ is the liquid density and μ is the fluid viscosity. The dimensionless axial velocity V_z / V_{tip} versus r/R is provided in Fig.4. The results of CFD work have been compared with Tsui *et al.* [24]. The same pattern can be seen for all Reynolds number for a non-Newtonian fluid. The maximum value of V_z / V_{tip} increases with an increase in the Reynolds number.

4. Results and discussion

The distribution of tangential velocity at different Reynolds numbers has been presented in Fig.5 and

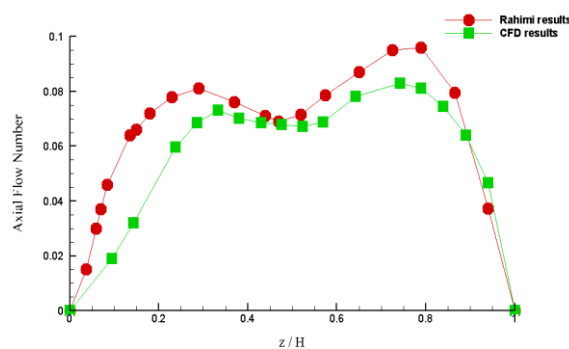


Fig.4. Comparison of the predicted dimensionless axial flow number with the data of Rahimiet al. [23].

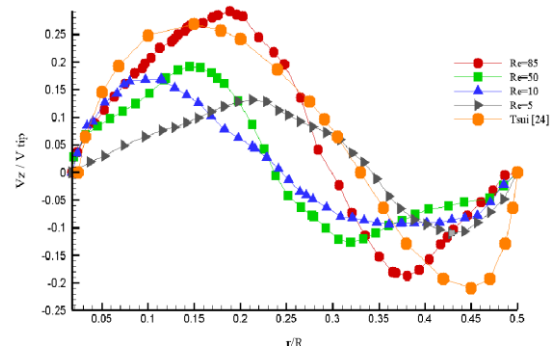


Fig.5.Dimensionless axial velocity at different Reynolds number for non-Newtonian fluid.

Fig.6. It is shown in Fig.5 that the tangential has a smoother pattern for Newtonian fluid than the non-Newtonian fluid. In the case of Newtonian fluid, variation of V_{θ} / V_{tip} in region where $0 < r/R < 0.5$ is moderate. But by approaching to the impeller, a sharp gradient is created where $0.5 < r/R < 0.8$. The maximum value of V_{θ} / V_{tip} is occurred where $0.8 < r/R < 0.85$ and then decreased until reaching the tank's wall. It can also be seen that the maximum value of V_{θ} / V_{tip} has a small shift to the left with an increase in the Reynolds number. It happens because the fluid between the outer impeller tip and tank wall is affected by the no-slip condition caused by tank wall. On the other hand, the momentum transfer between fluid layers happens more freely for the fluid between inner impeller tip and the shaft.

For non-Newtonian fluids, the behaviour is relatively complex. Fig.7 illustrates dimensionless tangential velocity at different Reynolds number for a non-Newtonian fluid. Where $0 < r/R < 0.5$, the change in V_{θ} / V_{tip} for the non-Newtonian fluid is higher than the Newtonian fluid because of the effect of viscous layers on each other. Considering Fig.7, where $0.5 < r/R < 0.75$, the sharp gradient

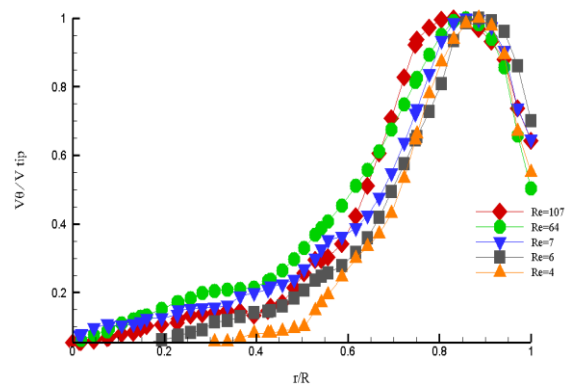


Fig. 6. Dimensionless tangential velocity at different Reynolds number for a Newtonian fluid

occurs. The maximum values of V_{θ}/V_{tip} have been seen in points where $0.75 < r/R < 0.9$ which is a wider area than the one of the Newtonian fluid. This phenomenon is caused by the viscous effect of the fluid layers close to the impeller tip on adjacent layer that is much greater than that of a Newtonian fluid. The non-Newtonian fluid layers perceived the momentum transfer of the impeller tip more than the Newtonian fluid layers. So, a decrease in V_{θ}/V_{tip} for the non-Newtonian fluid is less than the Newtonian one.

4.1 characteristics of kinetic energy

The kinetic energy (ke) was defined as follows:

$$Ke = \frac{1}{2} \rho v^2 \tag{6}$$

In which v is the velocity vector. Figure 8.compares the custom field function of kinetic energy (ke) of both Newtonian and non-Newtonian fluids at different Reynolds numbers in an axial slice that goes through the middle of the tank. Distribution of kinetic energy represents regions with different velocities. The maximum and the average of kinetic energy vary with the change in flow regime, therefore the same color for different Reynolds numbers have disparate values.

So, simulations were run in three regions: (i) $0 < Re < 10$, (ii) $10 < Re < 100$ and (iii) $100 < Re < 250$. In each region, a specific value was used to represent the boundary between stationary and moving zones. In all three cases, the interior region is shown in blue that represents the areas with lower velocities and the outer region close to impeller is displayed by yellow that represents the areas with higher velocities. To have detailed

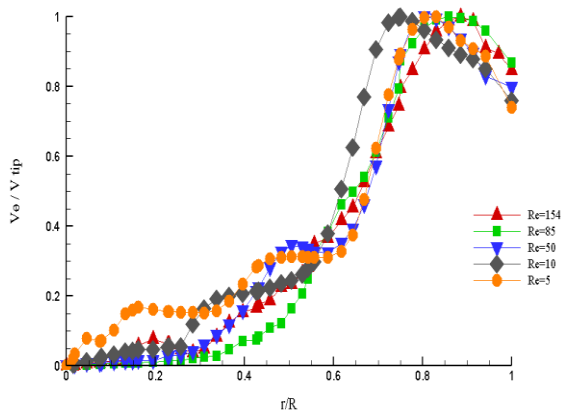


Fig.7.Dimensionless tangential velocity at different Reynolds numbers for a non-Newtonian fluid.

analyses for each region, it is needed to determine the exact value of kinetic energy which is valid for all runs in the region. According to this viewpoint, Figs. 8-10, illustrating the dimensionless stationary diameter versus Reynolds number, were prepared in which the dimensionless stationary diameter (di°) is the ratio of the diameter of stationary region (d_s) to tank diameter (D).

$$di^{\circ} = \frac{d_s}{D} \tag{7}$$

The results show that the diameter of stationary region depends on Reynolds number and type of the fluid.

The dimensionless diameter of stationary zone (di°) versus Reynolds number is plotted in Fig.8. It can be seen that in laminar region with Reynolds number close to one, the stationary region has a volume about 65 percent of the total volume for the Newtonian fluid and 58percent of the total volume for the non-Newtonian fluid. But, this percentage decreases with an increase in the Reynolds number. While the Reynolds number approaches to the transient values, a more reduction in the slop occurs. In the region with Reynolds number close to ten, the stationary region has just a volume of about 35 percent of the total volume.

It is shown in Fig.10 that the (di°) decreases with the increase in Reynolds number and the decreasing slop of Non- Newtonian fluid is greater than of Newtonian fluid by receding from laminar region. This pattern, seen in all three figures, is due to viscous effect of fluid layers at different Reynolds numbers. In laminar region, where $0 < Re < 10$, because of a lower velocity, the momentum transfer is in the lowest level and the two fluids have the most similar behaviours; therefore, both

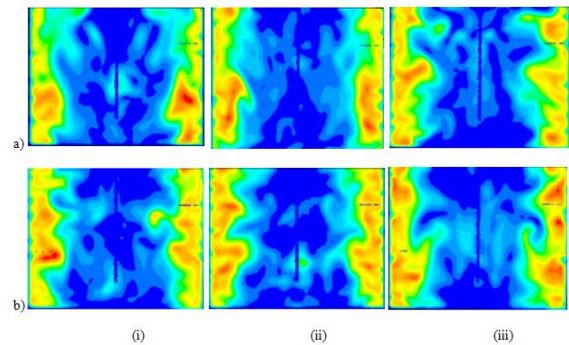


Fig. 8. Contours of custom field function of kinetic energy (ke) of fluid at different Reynolds numbers for (a) Newtonian fluid and (b) Non-Newtonian fluid.

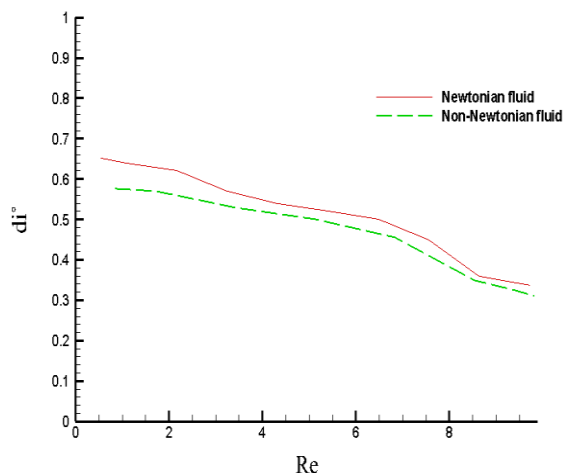


Fig. 9. The dimensionless diameter of stationary zone (di°) versus Reynolds number in laminar region.

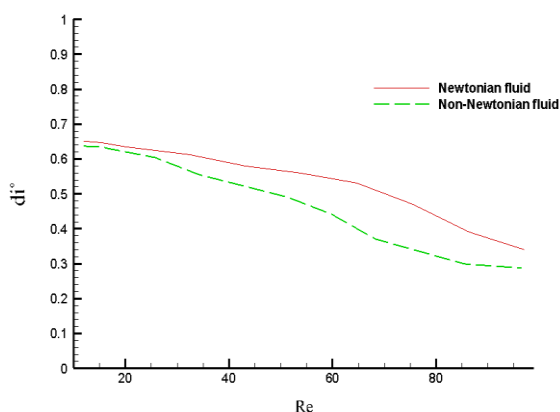


Fig. 10. The dimensionless diameter of stationary zone (di°) versus Reynolds number in transient region close to the laminar region.

diagrams have the same trend.

It is shown in Fig.10 that the (di°) decreases with the increase in Reynolds number and the decreasing slope of Non-Newtonian fluid is greater than of Newtonian fluid by receding from laminar region. This pattern, seen in all three figures, is due to viscous effect of fluid layers at different Reynolds numbers. In laminar region, where $0 < Re < 10$, because of a lower velocity, the momentum transfer is in the lowest level and the two fluids have the most similar behaviours; therefore, both diagrams have the same trend.

By increasing the Reynolds number above 20, where the secondary flow occurs, the differences between Newtonian and Non-Newtonian fluids' decreasing slope increase. These differences are more evident in the region where $Re > 50$. The dimensionless diameter of stationary zone has a higher reduction for Non-Newtonian fluid than the Newtonian fluid. It happens because the viscosity

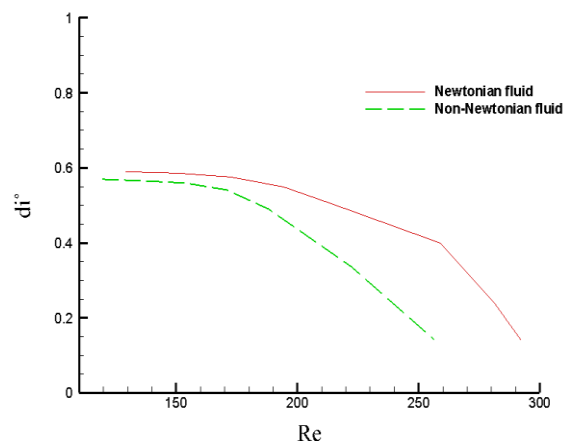


Fig. 11. The dimensionless diameter of stationary zone (di°) versus Reynolds number in transient region.

effect on adjacent layers in Non-Newtonian fluid is higher than the Newtonian fluid. So, the momentum transfer occurs by a greater number of layers that is farther from the impeller tip. Consequently, the stationary area has a smaller volume. Similar to Fig.8 and Fig.9, decreasing trend with increase in Reynolds number can also be seen in Fig. 10. But, a sharp decline occurred where $Re > 200$ and the difference between Newtonian and non-Newtonian fluids is maximum. This happens because of prevailing secondary flows in $Re > 200$ for Newtonian fluids [25, 26]. The results were compared with the literatures and they were in good agreement with Tsuiet *al.* [24] results which chose the value of 0.45 for dimensionless diameter of stationary zone for Reynolds number equal to 5.

5. Conclusions

The multi reference frames were used to simulate the impeller rotation in a mixing system. In order to use the MRF method, the calculation area should involve both stationary and moving zones. The accurate determination of boundaries of these two zones results in better mixing performance that can be determined by segregated area defined with different velocities. The kinetic energy function was used to determine both stationary and moving zones. The areas with kinetic energy close to zero were determined as the stationary zone and the remained area were determined as the moving zone. The results show that the dimensionless diameter of stationary zone reduced with an increase in the Reynolds number and because of higher viscous effects of non-

Newtonian fluid than that of the Newtonian fluid. This decrease is bigger for non-Newtonian fluids. As expected, the dimensionless diameter of stationary zone reduces as fluid viscosity increases. This can be investigated by further researches. The axial velocity and axial flow number were compared with literature for validation.

Acknowledgment

We are so grateful to Tsui for sending us his paper's data which was a great help in preparing this paper.

References

- [1]. P.J. Carreau, I. Patterson, C.Y. Yap, "Mixing of viscoelastic fluids with helical-ribbon agitators - I. Mixing time and flow patterns," *Can. J. Chem. Eng.* 54 (1976) pp. 135-142.
- [2]. S.M. Shekhar, S. Jayanti, "Mixing of Pseudoplastic Fluids Using Helical Ribbon Impellers," *AIChE J.* 49 (2003) pp. 2768-2772.
- [3]. M. Jahangiri, "Velocity distribution of helical ribbon impeller in mixing of polymeric liquids in the transition region," *Iranian Polymer J.* 16 (2007) pp. 731-739.
- [4]. M. Jahangiri, "Shear Rates in Mixing of Viscoelastic Fluids by Helical Ribbon Impeller," *Iranian Polymer J.* 17 (2008) pp. 831-341.
- [5]. K. Takahashi, Y. Takahata, T. Yokota, H. Konno, "Mixing of two miscible highly viscous Newtonian liquid in a helical ribbon agitator," *J. Chem. Eng. Japan.* 18 (1985) pp. 159-162.
- [6]. P. J. Carreau, R.P. Chhabra, J. Cheng, "Effect of rheological properties on power consumption with helical ribbon agitators," *AIChE J.* 39 (1993) pp. 1421-1430.
- [7]. G. Delaplace, J.C. Leuliet, V. Relandeau, "Circulation and mixing times for helical ribbon impellers. Review and experiments," *Experiments in Fluids.* 28 (2000) pp. 170-182.
- [8]. I. Ihejirika, F. Ein-Mozaffari, "Using CFD and Ultrasonic Velocimetry to Study the Mixing of Pseudoplastic Fluids with a Helical Ribbon Impeller," *Chem. Eng. Technol.* 30 (2007) pp. 606-614.
- [9]. W.I. Patterson, P.J. Carreau, C.Y. Yap, "Mixing with helical ribbon agitators, Part II. Newtonian fluids," *AIChE J.* 25 (1979) pp. 508-516.
- [10]. K.V. Vyakaranam, J.L. Kokini, "Advances in 3D Numerical Simulation of Viscous and Viscoelastic Mixing Flows," in: J.M. Aguilera, Simpson R, Welti-Chanes J, Bermudez Aguirre D, Baebosa-Canovas G (Eds.) *Food Engineering interfaces*, Springer Science, Business Media, (2011), pp. 19-44.
- [11]. P.M. Armenante, C. Luo, C.C. Chou, I. Fort, J. Medek, "Velocity profiles in a closed, unbaffled vessel: comparison between experimental LDV data and numerical CFD prediction," *Chem. Eng. Sci.* 52 (1997) pp. 3483-3492.
- [12]. D. Anne-Archard, M. Marouche, H.C. Boisson, "Hydrodynamics and Metzner-Otto correlation in stirred vessels for yield stress fluids," *Chem. Eng. J.* 125 (2006) pp. 15-24.
- [13]. J. Aubin, I. Naude, C. Xuereb, J. Bertrand, "Blending of Newtonian and Shear-Thinning Fluids in a Tank Stirred with a Helical Screw Agitator," *Cherd Trans. IChemE.* 78 (2000) pp. 1105- 1114.
- [14]. J. Aubin, I. Naude, C. Xuereb, "Design of Multiple Impeller Stirred Tanks for the Mixing of Highly Viscous Fluids Using CFD," *Chem. Eng. Sci.* 61 (2006) pp. 2913-2920.
- [15]. B. Letellier, C. Xuereb, P. Swaels, P. Hobbes, J. Bertrand, "Scale-up in laminar and transient regimes of a multi-stage stirrer, a CFD approach," *Chem. Eng. Sci.* 57 (2002) pp. 4617-4632.
- [16]. R. Sanjuan-Galindo, M. Heniche, G. Ascanio, P.A. Tanguy, "CFD investigation of new helical ribbon mixers bottom shapes to improve pumping," *Asia-Pac. J. Chem. Eng.* 6 (2011) pp.181-193.
- [17]. H. Ameer, M. Bouzit, M. Helmaoui, "Numerical study of fluid and power consumption in a stirred vessel with a Scsbs 6SRGT impeller," *Chem. Process Eng.* 32 (2011) pp.351-366.
- [18]. H. Ameer, M. Bouzit, "Agitation of Yield Stress Fluids by Two-Blade Impellers," *Canadian J. on Chem. Eng. Technol.* 3 (2012) pp. 93-99.
- [19]. H. Ameer, M. Bouzit, M. Helmaoui, "Hydrodynamic study involving a maxblend impeller with yield stress fluids," *J. Mech. Sci. Technol.* 26 (2012) pp. 1523-1530.
- [20]. S. Youcefi, M. Bouzit, H. Ameer, Y. Kamla, A. Youcefi, "Effect of some design parameters on the flow fields and power consumption in a vessel stirred by a Rushton Turbine," *Chem. process Eng.* 34 (2013) pp. 293-307.
- [21]. J.Y. Luo, I. Issar, A.D. Gosman, "Prediction of impeller induced flows in mixing vessels using multiple frames of reference," *Proceeding Institution Chem. Eng.* 136 (1993) 549-556.
- [22]. M. Zhang, L. Zhang, B. Jiang, Y. Yin, X. Li, "Calculation of Metzner Constant for Double Helical Ribbon Impeller by Computational Fluid Dynamic Method," *Chinese J. Chem. Eng.* 16 (2008) pp. 686-692.
- [23]. M. Rahimi, A. Kakekhani, A. AbdulazizAlsairafi, "Experimental and computational fluid dynamic (CFD) studies on mixing characteristics of a modified helical ribbon impeller," *Korean J. Chem. Eng.* 27 (2010) pp.1150-1158.
- [24]. Y. Tsui, Y. Hu, Eng. "Flow characteristics in mixers agitated by helical ribbon blade impeller," *Application of Computational Fluid Mechanics.* 5 (2011) pp.416-429.
- [25]. L.W. Adams, "Experimental and computational study of non-Turbulent flow regimes and cavern formation of non-Newtonian fluids in a stirred tank," PhD thesis, Birmingham, 2009, B15 2TT.
- [26]. V.V. Chavan, R.A. Mashelkar, "Mixing of viscous Newtonian and non-Newtonian fluids," in: A.S. Mujumdar (Ed.) *Advances in Transport Processes*, Wiley Eastern/Wiley Halsted, 1980, pp. 210-252.

تعیین مرز ناحیه سکون در روش قاب مرجع چندگانه در یک سیستم اختلاط دارای همزن با پره حلزونی با استفاده از دینامیک سیالات محاسباتی

مریم صناعی مقدم^۱، منصور جهانگیری^{۲*}، فرامرز هرمزی^۳

۱. دانشکده مهندسی شیمی، نفت و گاز، دانشگاه سمنان، سمنان

۲. دانشکده مهندسی شیمی، نفت و گاز، دانشگاه سمنان، سمنان

۳. دانشکده مهندسی شیمی، نفت و گاز، دانشگاه سمنان، سمنان

اطلاعات مقاله	چکیده
دریافت مقاله: ۷ اردیبهشت ۱۳۹۳ پذیرش مقاله: ۳۱ تیر ۱۳۹۳	
واژگان کلیدی: CFD, MRF, پره حلزونی، اختلاط، مایع غیر نیوتنی.	روش فریم های متعدد مرجع (MRF)، مناسبترین روش برای شبیه سازی چرخش پره همزن در سیستم های اختلاط است. تعیین دقیق محدوده های ثابت و متحرک در روش MRF منجر به دستیابی به نتایج دقیق در عملکرد سیستم اختلاط خواهد شد. در این تحقیق، حجم داخلی سیستم اختلاط به دو ناحیه تقسیم شده است. از مقادیر انرژی جنبشی برای مشخص کردن نواحی دارای سرعت های مختلف استفاده شده است. مناطق با سرعت پایین، نزدیک به صفر به عنوان ناحیه ثابت و نواحی با سرعت بالاتر به عنوان منطقه در حال حرکت در نظر گرفته شد. از نسبت ابعادی استاندارد برای سیستم اختلاط استفاده شده است. جهت اعتبار سنجی، سرعت محوری و عدد جریان محوری با نتایج مقالات مقایسه شد. مقادیر قطر بدون بعد ناحیه سکون در اعداد رینولدز مختلف، برای مایعات نیوتنی و غیر نیوتنی بررسی شد که در توافق با مقادیر مورد استفاده در مراجع است. نتایج نشان می دهد که قطر بدون بعد ناحیه سکون با افزایش عدد رینولدز کاهش می یابد.